Vitamins as Active Agents for Highly Emissive and Stable Nanostructured Halide Perovskite Inks and 3D Composites Fabricated by Additive Manufacturing

Ileana Recalde, Andrés. F. Gualdrón-Reyes,* Carlos Echeverría-Arrondo, Alexis Villanueva-Antolí, Jorge Simancas, Jhonatan Rodriguez-Pereira, Marcileia Zanatta, Iván Mora-Seró,* and Victor Sans*

Supporting Information

Vitamins as active agents to Achieve Highly Emissive and Stable Nanostructured CsPbI₃ Inks and 3D Composites Fabricated by Additive Manufacturing

Ileana Recalde,[1#] Andrés. F. Gualdrón-Reyes,[1,2,#,*] Carlos Echeverría-Arrondo,[1]

Alexis Villanueva-Antolí,[1] Jorge Simancas,[1] Jhonatan Rodriguez-Pereira,[3,4] Marcileia Zanatta,[1]

Iván Mora-Seró[1,*] and Victor Sans[1,*]

[1]Institute of Advanced Materials (INAM), Universitat Jaume I (UJI), Avenida de Vicent Sos Baynat, s/n, 12071 Castelló de la Plana, Castellón, Spain.

[2]Facultad de Ciencias, Instituto de Ciencias Químicas, Isla Teja, Universidad Austral de Chile, 5090000, Valdivia, Chile.

[3]Center of Materials and Nanotechnologies, Faculty of Chemical Technology, University of Pardubice, Nam. Cs. Legii 565, 53002 Pardubice, Czech Republic.

[4]Central European Institute of Technology, Brno University of Technology, Purkyňova 123,612 00 Brno, Czech Republic.

Corresponding authors: gualdron@uji.es, sero@uji.es, sans@uji.es

#Authors contributed equally to this work

Experimental section

Synthesis of perovskite nanocrystals (PNCs)

CsPbX₃ perovskite NCs were obtained by a hot-injection synthetic protocol through stoichiometrically mixing both the Cs-oleate and PbI₂ solutions as described elsewhere with some modifications.[1] To obtain the Cs-oleate solution, 0.61 g Cs₂CO₃ (202126, 99.9 %, Sigma-Aldrich) and 2 mL oleic acid (OA, 364525, 90 %, Sigma-Aldrich) were mixed in 30 mL of 1 octadecene (1-ODE, O806, 90 %, Sigma-Aldrich) into a 50 mL-three neck flask under vacuum for 30 min at 120 °C and kept under vacuum for 30 min. The mixture was heated to reach 150 °C under N₂-purge to dissolve the Cs₂CO₃ completely. In order to prevent the Cs-oleate precipitation to produce Cs₂O, the resultant solution was kept at 120 °C under vacuum.

In order to synthesizing pure CsPbI₃, 1 g PbI₂ (ABCR; AB111058, 99.999%) was mixed with 50 mL 1-ODE into a 100 mL-three neck flask and then degasified at 120 °C under vigorous stirring for 1

h. Then, 5 mL of each preheated OA and oleylamine (HT-OA100, 98 %, Sigma-Aldrich) were added to the flask at heated again at 170 °C. Simultaneously, 4 mL of preheated Cs-oleate was swiftly injected at this temperature into yellow PbI_2 solution, obtaining a red precipitate in the colloidal solution. Immediately, the flask was immersed into an ice bath for 5 s to quench the reaction. For isolating process, the dispersed NCs were centrifuged at 5000 rpm for 5 min with methyl acetate (MeOAc, 296996, 99.5%, Sigma Aldrich) (all final NCs liquor washed with 120 mL MeOAc). The precipitated NCs were recovered from supernatant and re-dispersed in 5 mL of hexane (CHROMASOLV, 34859, 99.7 %, Honeywell). $CsPbI_3$ NCs solution was dried and redispersed in hexane to obtain a final concentration of 100 mg/mL. As-prepared PNCs are named P1 in main text). Then, PNCs were aged by exposing them to ambient air at room temperature (~20 ℃), and 30% relative humidity under dark conditions. Aged PNCs were named as P2 in the main text. With the purpose to analyze the effect of tocopherol (α-TCP, 97% Alfa Aesar) on the photophysical properties and the stability of as-prepared and aged $CsPbI_3$ PNCs, several concentrations of the vitamin were added to 0.3 g of $CsPbI_3$ at 100 mg/mL. $CsPbBr_3$ and $CsPbCl_{3-x}Br_x$ PNCs were synthesized by following the above-described procedure, by introducing 0.8 g $PbBr_2$ (AB202085, 99.998 %, ABCR) and the corresponding Cl:Br composition (1:1) ($PbCl_2$, AB202087, 99.999%, ABCR) were added to the mixture reaction.

Preparation of Stable and Highly Luminescent PNCs–Polymer Composite Films

Monomers buthylacrylate (BA, Sigma-Aldrich) and isobornyl acrylate (IBA, Sigma-Aldrich), used as the matrix in composite specimens and 1,4-Butanediol diacrylate (DBA, Sigma-Aldrich) used as crosslinker agent, as well as the UV-initiator diphenyl(2,4,6-trimethylbenzoyl)phosphine oxide (TPO, Sigma-Aldrich), were employed without further purification. In an opaque vial, a solution of $CsPbI_3$ NCs in toluene was dried under vacuum for 3 min at 175 ppm and at room temperature to remove the solvent. For UV-curing purpose, $CsPbI_3$ NCs acrylic composite was prepared according to the following procedure: Once dried, the $CsPbI_3$ NCs was dispersed in IBA at room temperature with continuous and soft stirring until a clear dissolution was obtained. α-TCP percentages were added followed by vigorous vortex mixing to obtain a homogeneous mixture. Preselected weight of BA monomer was then added to the mixture with a final soft stirring. The acrylic monomers were mixed with the required amount of the crosslinker agent and photoinitiator (PI). The mixtures were kept under constant magnetic stirring for 30 min. Then, the obtained dispersions were refrigerated for almost 15 min prior to cure. Chilled solutions were coated on glass slides, using a wire wound applicator (film thickness about 50 μm), and placed inside 1 mm x 2 mm rectangular transparent moulds and then exposed to the UV radiation provided by a UV-Fore Cure unit, 405 nm light, with heating system curing control (Formlabs, USA) working in static conditions. Modified acrylic monomeric matrices containing 0-20 mol% the crosslinker agent and 0-5.0 wt% dry perovskite were mixed with 0.5-2.5 wt% of UV-initiator. A set of clear glass moulds, each containing about 1 mL of chilled mixture, were placed in a UV-cabin at curing temperature (selected within the range from 30℃ to 60℃). The moulds were removed from the cabin

after selected time of reaction (40 min to 90 min). The obtained UV-cured films were peeled off from the glass slides and mould and used for the different characterizations. Flowchart 1 show the schematic procedure to the preparation of stable and highly luminescent $CsPbI_3$ NCs–Polymer composite films. The prepared polymeric samples were named according to the percentage of each component in the mixture, following the naming (BA:IBA: DBA:PI:PNCs:α-TCP).
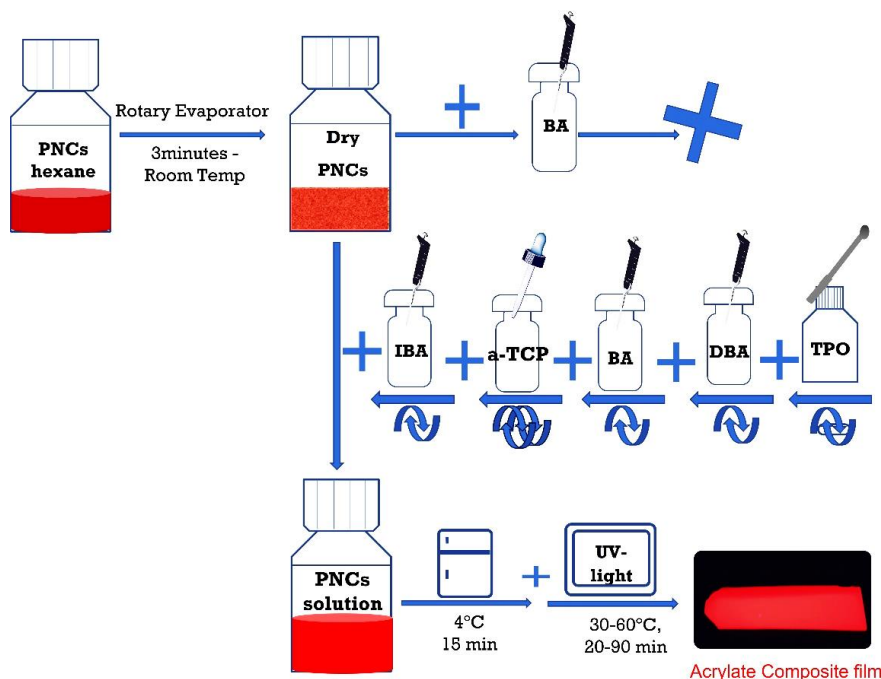
Flowchart 1. Sequence of preparation of $CsPbI_3$ PNCs-acrylic composites films

The resulting polyacrylate films containing different percentage (wt%) of n-butyl acrylate and isobornyl acrylate, in presence or not of $CsPbI_3$ PNCs and tocopherol, were characterized. The best results were obtained for polymeric material with 7 wt% of crosslinker and 1.5 wt% of UV-initiator, 1.5 wt% of $CsPbI_3$ PNCs in presence 2.5 wt% α-TCP (0.15 M into nanocrystals). For carrying out the printing process, an Elegoo Mars 2 Pro LCD printer was used. The perovskite dispersed in the acrylate formulation was transferred to the printing pool and the following printing parameters were used: 0.025 mm layer height; 15 seconds / layer exposure time; 60 mm/min lifting speed. After printing, the model was recovered and further cured in a FormCure UV curing chamber for 60 min at 45ºC.

Theoretical calculations

Nanoparticles and ligands were theoretically studied with CP2k, a software package conceived to perform density functional theory (DFT) calculations based on a mix of plane waves and Gaussian functions.[2, 3] In particular, we used the Perdew-Burke-Ernerhof (PBE) approach to generate the pseudopotentials,[4] a double-zeta valence basis set augmented with polarization functions (DZVP), and spin polarization. The atomic positions in all the systems were geometrically relaxed with this code until

the forces on the individual nuclei became smaller than 0.003 Ha/a$_0$, where a 0 is the Bohr radius. In addition, cubic nanocrystals were separated from each other by 12 Å of void space so as to minimize reciprocal interactions. The electronically balanced chemical formula of the net nanoparticle, of 31 Å of size, is $(CsPbI_3)_{125}$ $(CsI)_{75}$, which yields a clean band gap free of trap states from the surface.[3, 5]

Characterization of the CsPbI$_3$ PNCs colloidal solutions

The morphology of PNCs was analyzed through high-resolution transmission electron microscopy (HR-TEM) by using a LaB6 Jeol JEM 2100plus, with applied bias of 200 kV, while the crystalline structure for the PNCs was observed by selective area electron diffraction (SAED) patterns. The average particle size of PNCs was obtained from the TEM images with ImageJ software. X-ray diffraction (XRD) profiles of the materials were obtained by using a D4 Endeavor diffractometer from Bruker-AXS, using a Cu Kα radiation source (λ = 1.54056 Å). Steady state- and time-resolved photoluminescence (PL) measurements were conducted on PNCs-composites and colloidal solutions through photoluminescence spectrophotometer (Fluorolog 3-11, Horiba). An excitation wavelength of 420 nm was used to perform the steady state PL. The concentration of the samples was fixed to 2 mgmL^{-1} in hexane, using a quartz cuvette of 10 x 10 mm. Time-resolved PL measurements were carried out at 405 nm pulsed laser (NanoLED-405L, <100 ps of pulse width, 1 MHz frequency). The absolute photoluminescence quantum yield (PLQY) of the PNCs was estimated through a Hamamatsu PLQY Absolute QY Measurement System C9920-02, equipped with an integrating sphere, at an excitation wavelength of 400 nm. Before conducting the measurements, absorbance was fixed in an interval range around 0.4-0.5, being these values adequate to achieve the maximum PLQY in the samples. Surface chemical composition and electronic state of PQDs were determined by X-ray Photoelectron Spectroscopy (XPS, ESCA-2R, Scienta-Omicron). Spectra were recorded using monochromatic Al Kα = 1486.6 eV. The following sequence of spectra were recorded: survey spectra, C 1s, Pb 4f, I 3d, O 1s, N 1s. The survey and high-resolution spectra were recorded at a pass energy of 150 and 20 eV, respectively. Binding energy scale was referenced to adventitious carbon (284.8 eV). CasaXPS processing software (Casa software Ltd) was used to analyze the data and the quantitative analysis was made using sensitivity factors provided by the manufacturer. Nuclear Magnetic Resonance (NMR) spectroscopy were performed on PNCs colloidal solutions using a Bruker Avance III HD spectrometer operating at a 1H frequency of 400 MHz, at 298 K. ^{1}H spectra were processed in MestReNova software.

Characterization of the CsPbI$_3$-composites

Glass transition temperature (Tg) of the polymeric samples was evaluated using Differential Scanning Calorimetry (DSC). DSC measurements were performed with a Mettler Toledo DSC2 and the results were analyzed using STARe software version 6.01. The DSC was calibrated with high purity indium and zinc. Six to eight milligrams of samples were weighed into DSC aluminum pans and sealed with holed aluminum lids, in all experiments three replicates were analyzed. The experiments were conducted

under a nitrogen flow of 50 mL/min. All the samples were subjected to a dynamic DSC scan from -70 to 250 ℃ at 10 C/min to determine the glass transition temperature of the cured material. The temperature corresponding to the onset of the transition was taken as the Tg.
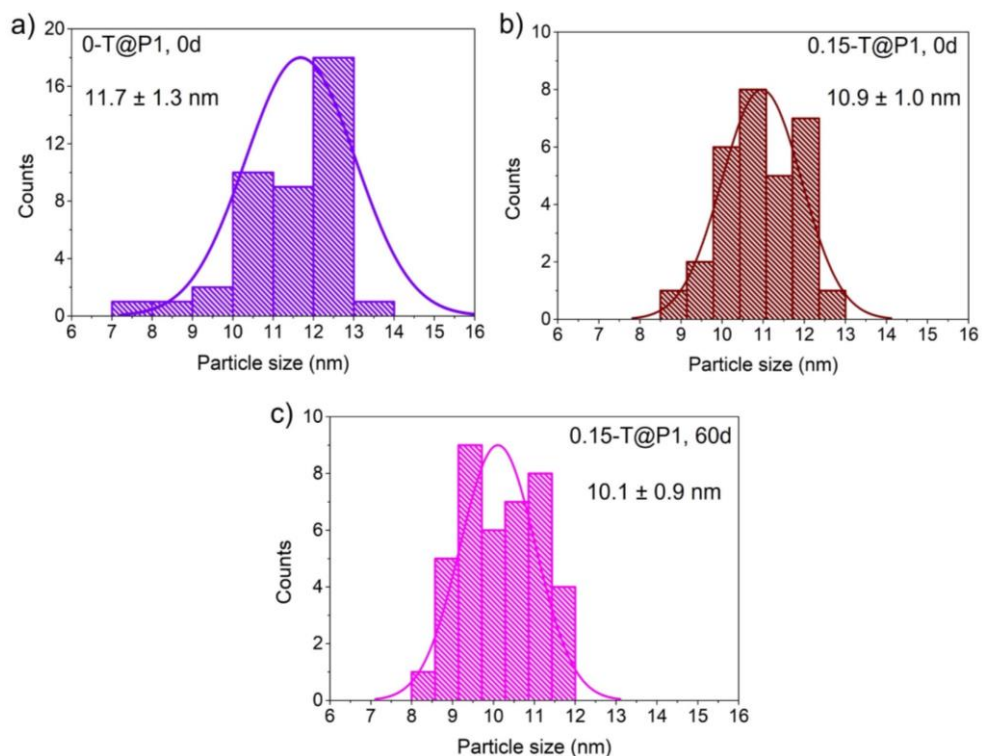

Figure S1. Histograms for estimating the particle size of (a) 0-T@P1 and (b) 0.15-T@P1 samples at day 0, (c) 0.15-T@P1 sample after 60 days aging.
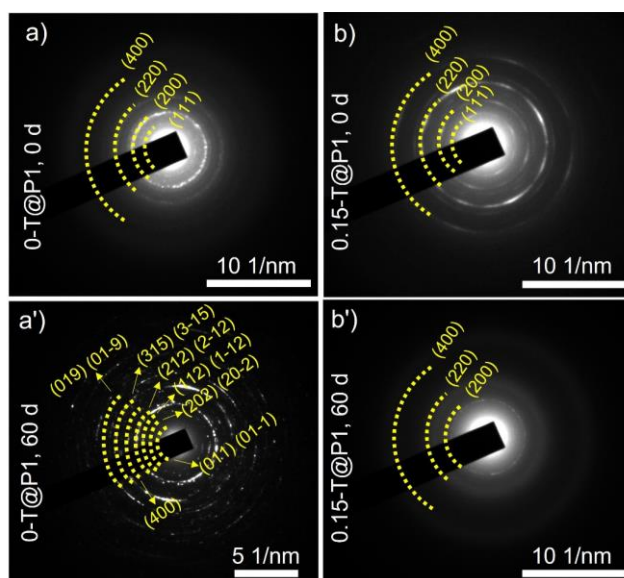

Figure S2. Selected area diffraction SAED patterns obtained with HRTEM for (a,a') 0-T@P1 and (b,b') 0.15-T@P1 samples at (a,b) day 0, and (a',b') after 60 days of aging.

α-to-δ phase transition in pristine CsPbI₃ PNCs

Considering that pristine CsPbI$_3$ PNCs (Figure S3a) is prone to suffer the loss of surface ligands through aging process or/and after purification step with polar solvents such as methyl acetate,[6] this effect promotes the lattice distortion into the perovskite, breaking the symmetry.[7] The octahedral tilting generates a change in the morphology, emerging the presence of hexagonal-type nanoparticles (showing a non-active orthorhombic phase) mixed with nanocubes (Figure S3b). This change produces a progressive quenching of optical properties of the material (Figures S3c,d). Interestingly, this structural deformation produces a dipolar moment in the system, initiating the self-assembly of nanocrystals in a rectilinear direction, decreasing the surface energy.[8] This can explain the eventual formation of nanowires after long time of aging.
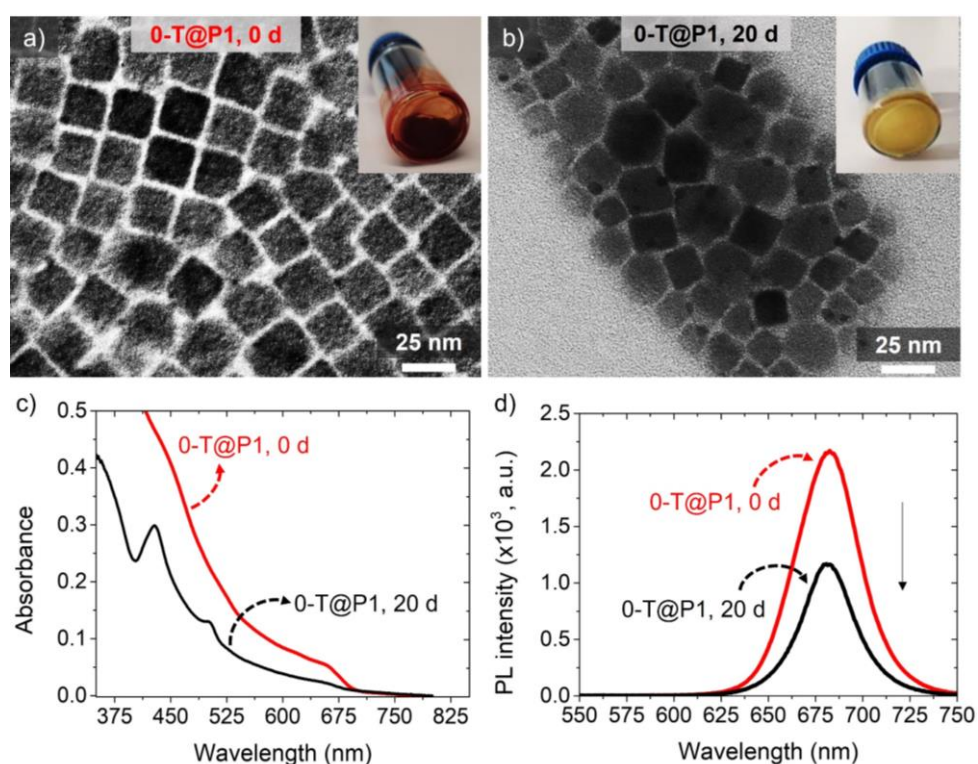

Figure S3. Typical TEM image of 0-T@P1 (a) at 0 day and (b) after 20 days of aging. Insets of Figure S2 show the photograph of the (a) as-prepared PNCs sample and (b) with a partial α-to-δ phase transformation.
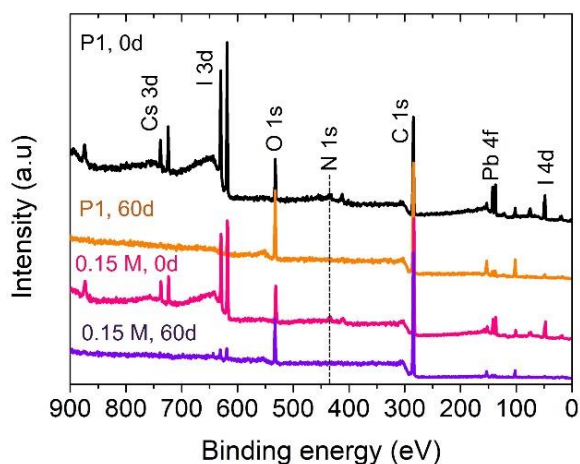
Figure S4. XPS survey spectra for 0-T@P1 (P1) and *X*-T@P1 (*X* = 0.15 M) samples under different time of aging (0 and 60 days).

Table S1. Chemical atomic composition of 0-T@P1 and 0.15-T@P1 samples under different time of aging (0 and 60 days).

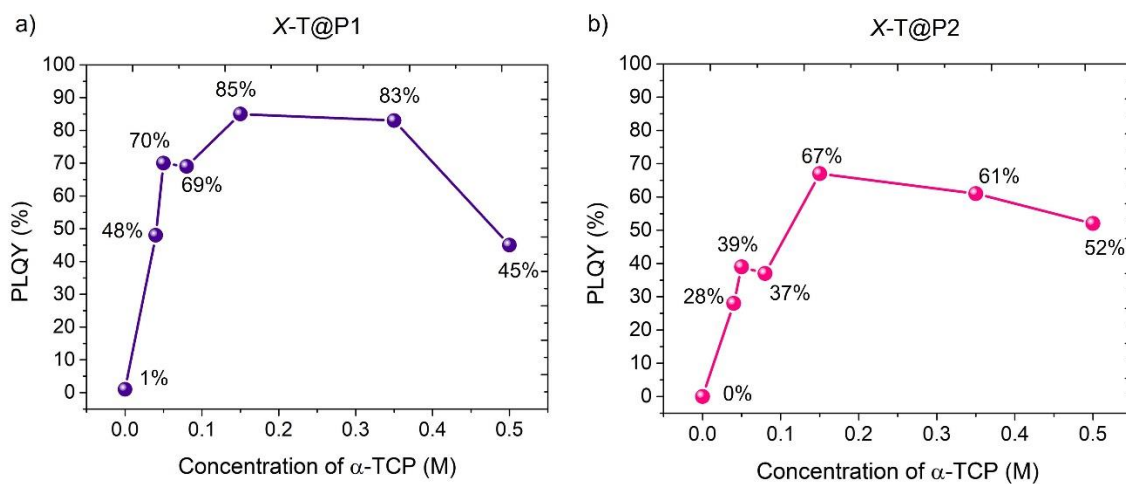| Perovskite	C (at.%)	O (at.%)	I (at.%)	Pb (at.%)	Cs (at.%)	N (at.%)	I/Pb	O/(I+O)	O/(O+Pb)	Δ O/(I+O)	Δ O/(O+Pb)
0-T@P1, 0 d	79.83	10.12	5.37	1.53	1.32	1.82	3.51	0.65	0.87	-	-
0-T@P1, 60 d	80.65	17.90	0.48	0.19	0.07	0.71	2.53	0.97	0.99	0.32	0.12
0.15-T@P1, 0 d	83.97	10.09	3.47	0.97	0.83	0.67	3.58	0.74	0.91	-	-
0.15-T@P1, 60 d	88.37	11.11	0.34	0.10	0.09	-	3.40	0.97	0.99	0.23	0.08

Figure S5. PLQY of (a) *X*-T@P1 and (b) *X*-T@P2 colloidal solutions by varying the concentration of α-TCP after 60 days of aging.
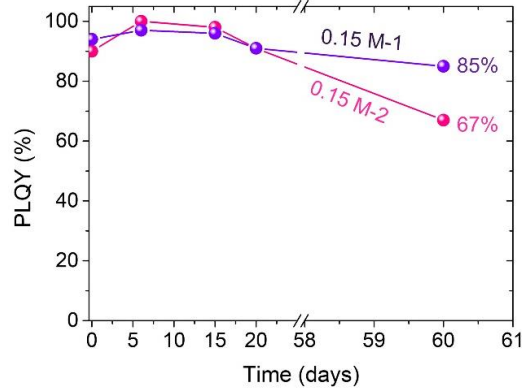
Figure S6. Comparison of stability in *0.15*-T@P1 (purple line) and *0.15*-T@P2 (pink line) colloidal solutions, after 60 days of aging.
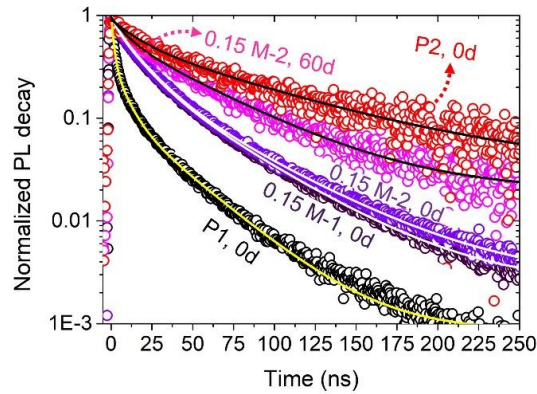

Figure S7. Time-resolved PL decay measurements of *X*-T@P1 and (b) *X*-T@P2 colloidal solutions in absence and presence of 0.15 M α-TCP at day 0 and after 60 days. Solid lines correspond to fitting the PL decays through a bi-exponential equation, $PL = y_0 + A_1 e^{-x/\tau_1} + A_2 e^{-x/\tau_2}$.

Table S2. Determination of radiative and non-radiative recombination decay rate constants, k_r and k_{nr}, respectively by fitting the time-resolved PL decays of the fresh and aged CsPbI$_3$ PNCs, in absence and presence of α-TCP from Figure S5 to a bi-exponential function $PL = y_0 + A_1 e^{-x/\tau_1} + A_2 e^{-x/\tau_2}$. Expressions used in the calculations: $\tau_{avg} = (\Sigma A_i \tau_i^2 / \Sigma A_i \tau_i)$, $\tau_{avg} = 1/(k_r + k_{nr})$ and $k_r = (PLQY/\tau_{avg})$.[9] PLQY values were used in 0-1 range.

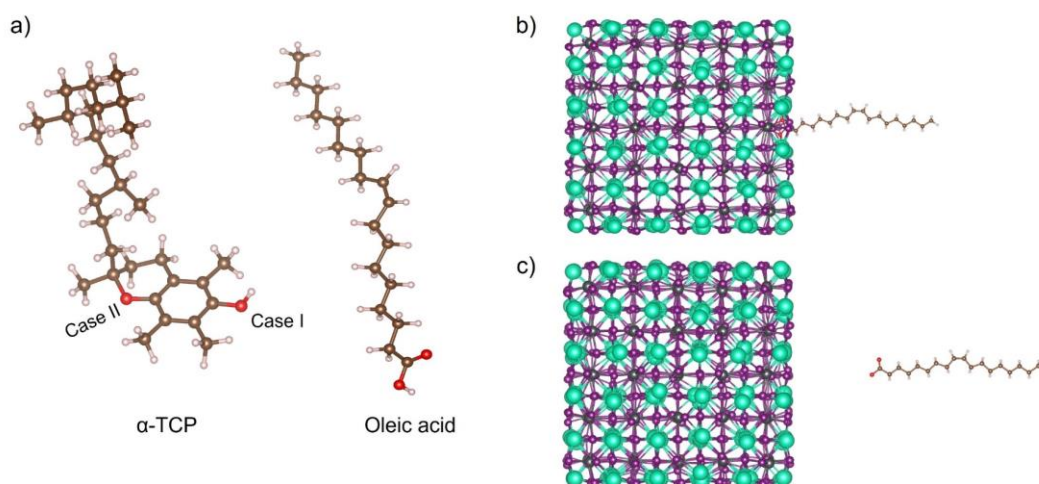| Perovskite sample	A_1 (%)	τ_1 (ns)	A_2 (%)	τ_2 (ns)	PLQY	τ_{avg} (ns)	k_r (10^7 s^{-1})	k_{nr} (10^7 s^{-1})	k_{nr}/k_r
P1, 0d	0.67	3.81	0.33	23.80	0.91	10.41	8.74	0.86	0.099
0.15 M-1, 0d	0.65	64.3	0.35	14.28	0.94	46.80	2.01	0.13	0.064
0.15 M-2, 0d	0.64	66.45	0.36	16.72	0.92	48.54	1.90	0.16	0.087
0.15 M-2, 60d	0.59	125.82	0.41	25.04	0.67	84.50	0.79	0.39	0.49
P2, 0d	0.54	200.80	0.46	39.40	0.48	126.55	0.38	0.41	1.08

Figure S8. (a) Atomic structures of α-TCP and oleic acid molecules after geometrical relaxation performed with CP2K, where the red dots represent oxygen atoms. Atomic representation of (b) a cubic $CsPbI_3$ nanocrystal (3.1 nm) with an oleic acid ligand on its surface, and (c) the same crystal and molecule without contact, far apart from each other (12 Å of void to minimize interactions).

Differential Scanning Calorimetry (DSC) measurements

The experimental values of the glass transition temperatures for the sample with α-TCP shows that addition of the vitamin reduces the maximum glass transition temperature in 20 ℃ approximately in all work polymeric systems studied, due to plasticization. For the sample 0-100 with α-TCP, the value of the Tg onset decrease until 25.73 ℃ (Tg Inflect Pt=50.44℃) and for the sample 10-90 with α-TCP the onset Tg value was 20.86 ℃ and the Tg (Inflect Pt was 32.10 ℃). Figure S7 shows representative DSC thermograms of the cured binary mixtures containing 0 and 10 wt% of IBA. All the DSC curves showed a typical glass transition platform, i.e., without any obvious endothermic melting peak occurring.
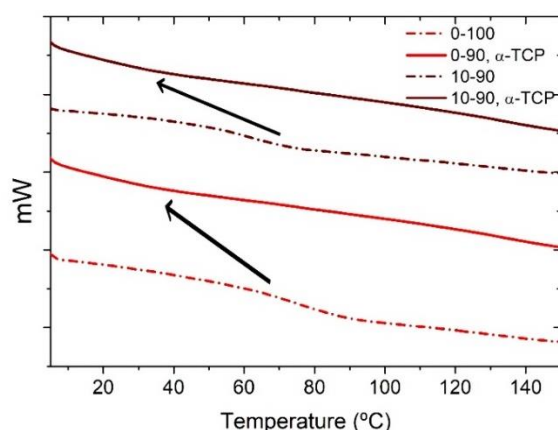

Figure S9. DSC thermograms of polyacrylic samples with 7 wt% of crosslinker, 1.5 wt% of UV-initiator, 1.5 wt% of $CsPbI_3$ PNCs and 2.5 wt% α-TCP (0.15 M in the nanocrystal solution) after cure at 50 ℃ for 60 min.
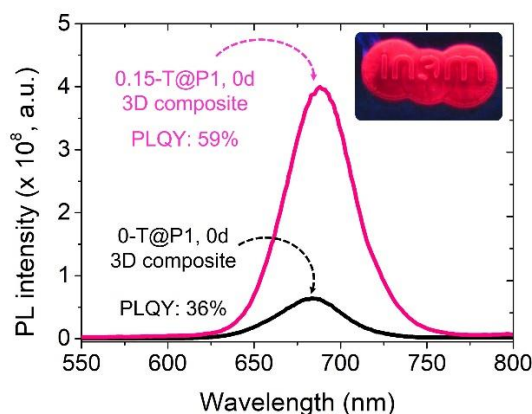
Figure S10. Effect of α-TCP on the PL features of as-prepared 0-T@P1 and 0.15-T@P1 acrylic composites at day 0. Composites contain 1.5 wt% of $CsPbI_3$ PNCs in presence and absence of 0.15 M α-TCP.

^{1}H-NMR characterization of $CsPbI_3$ colloidal solutions and 3D acrylate composites

With the purpose to obtain information about the surface chemistry of PNCs colloidal solutions before and after the addition of α-TCP, materials were characterized through ^{1}H NMR (Nuclear Magnetic Resonance) spectroscopy. We excluded the presence of 1-ODE as this chemical is a non-coordinating solvent and does not take part in the reaction but generates extra peaks in the corresponding ^{1}H NMR spectra. We have also conducted the ^{1}H NMR analysis to a mixture OA (0.25 M)/OLA (0.25 M), and then to a α-TCP sample for comparative purposes. Figure 4f in the main text exhibits the typical structures of the capping ligands and the corresponding ^{1}H NMR chemical shifts of each hydrogen position (denoted by numbers). In this way, the triplets at δ= 5.34, 2.76, 2.15 and 2.03 ppm present in the mixture are assigned to vinylene-H from the OA (8,9) and OLA (8',9'), CH_2 vicinal to vinylene groups (7,10) (7',10') and CH_2 near to COO^- (1) and NH_3^+ (1') funcionalities, respectively.[1, 10] At this point, the formation of oleylammonium oleate as the main ligand to carry out the PNCs stabilization is reached (blue spectra). By studying the ^{1}H NMR signals obtained from the as-prepared $CsPbI_3$ PNCs (red spectra), the vinylene protons maintain the same chemical shift, however methylene protons (1) near to COO^- group moves downfield, while decrease the intensity of the triplet for CH_2 near to NH_3^+. The change in the chemical shift of signal 1 can be attributed to its proximity to the PNCs surface, indicating the expected interaction between COO- and the perovskite. Furthermore, the washing process with MeOAc gives place to the detachment of capping ligands, for instance, oleylammonium iodide (OLAm-I), being the explanation to reduce the CH_2-close-to-NH_3^+ signal. In addition, in the PNCs sample, a extra signal is observed at δ= 1.95 ppm, corresponding to MeOAc from the washing procedure.[11] The appearance of this signal indicate that MeOAc is also pivotal to passivate halide vacancies from the PNCs surface, supporting the PNCs stabilization.

Then, after the addition of α-TCP to the PNCs colloidal solutions (brown spectra), we evidenced a change in the chemical environment, as new signals appeared. The typical NMR spectra of α-TCP (orange spectra) show the following signals: at δ= 4.16 (OH , 1''), 2.60, 2.15, 2.11, (CH$_3$ of signals 2'', 3'', 4''), 1.78 (6'') 1.53 (8'') and 1.23 (7'') ppm..[12] Additional NMR (between 0.9 to 1.6 ppm) signals correspond to CH$_2$ and CH$_3$ of the alkyl chain.[12] The above chemical shifts are also shown in the PNCs colloidal solution in presence of α-TCP, keeping the characteristic signals of OA/OLA observed in the materials absence of the vitamin. Interestingly. the peak associated to H-bonded to O disappeared from the NMR spectrum, and a broad signal at δ= 3.32 ppm emerges. Accordingly, this result indicates the deprotonation of phenolic OH from α-TCP, giving place to the formation of the phenolate species, responsible to promote the PNCs surface passivation. Attending to the fact that the resonances of CH$_2$ and CH$_3$ components near to epoxy ring from α-TCP appears unchanged, we can claim that oxygen from the epoxy functionality does not participate in the ligand passivation process, which is in good agreement with theoretical calculations.

On the other hand, to provide an explanation about how the addition of acrylates (BA and IBA) to the *X*-T@P samples can increase the PL properties of the final composite, we conducted ^{1}H-NMR analysis to different PNCs-acrylate formulation, observing their characteristic chemical shifts. In this way, the typical NMR spectrum of BA (Figure S10a) exhibits main signals at δ= 6.30, 6.07, and 5.75 ppm corresponding to the protons bonded to C=C (1*,2*,3*), while resonances at δ= 4.10, 1.59, 1.34 and 0.89 ppm are ascribed to protons from CH$_2$ (4*, 5*, 6*) and CH$_3$ composing the butyl substituent group (7*), respectively.[13, 14] In the case of IBA (Figure S10b), signals at δ= 6.26, 6.04, 5.75, are associated to hydrogens bonded to C=C (1**,2**,3**), while resonances at δ= 4.70 (4**), 1.82 (5a**), 1.79 (5b**), 1,76 (6**), 1.69 (7a**), 1.52 (8a**), 1.13 (8b**), 1.08 (7b**), and 0.86 (9**) ppm are related to protons from cyclohexyl ring. Then, signals at δ= 0.98 (10a**) and 0.83 (10b**) ppm are ascribed to protons in CH$_3$ component from isobornyl functionality.[13, 14] After combining separately BA, IBA, and a BA/IBA mixture (molar ratio 1:9) with α-TCP in presence and absence of PNCs, it was expected to evidence the main contributions of each monomer, taking into account that *X*-T@P is embedded into an acrylate matrix.

Nevertheless, we were able to observe changes in the main resonances of the *X*-T@P inks, for instance, one of the singlets corresponding to CH$_3$ (3'',4'') from the phenolic ring become a doublet, with a upfield shift to δ= 2.05 and 2.03 ppm for each peak, respectively. This feature indicates that both CH$_3$ present a discrepancy in the inductive effect provided by the chemical environment, promoting between their protons a different spin-spin coupling (two different kind of protons). Then, the triplet attributed to CH$_2$ into epoxy ring, near to aromatic functionality (5''), also shows an upfield shift, δ= 2.53 ppm. Accordingly, it is possible to suggest that epoxy ring can be opened in presence of BA and IBA. Moreover, the presence of the signal associated to protons bonded to C=C in BA (1*,2*,3*) and IBA (1**,2**,3**), indicates that acrylate functionality from monomers is involved into the chemical environment of the *X*-T@P-acrylate samples. These results indicate that acrylates mediate the epoxy

ring cleavage to produce alcoholate species, which is in good agreement with the theoretical calculations. This interaction is the first step to provide new capping ligands such as the formation of tocopheryl hydroquinone (or quinone), which would be attractive to analyze in future works of PNCs stabilization.
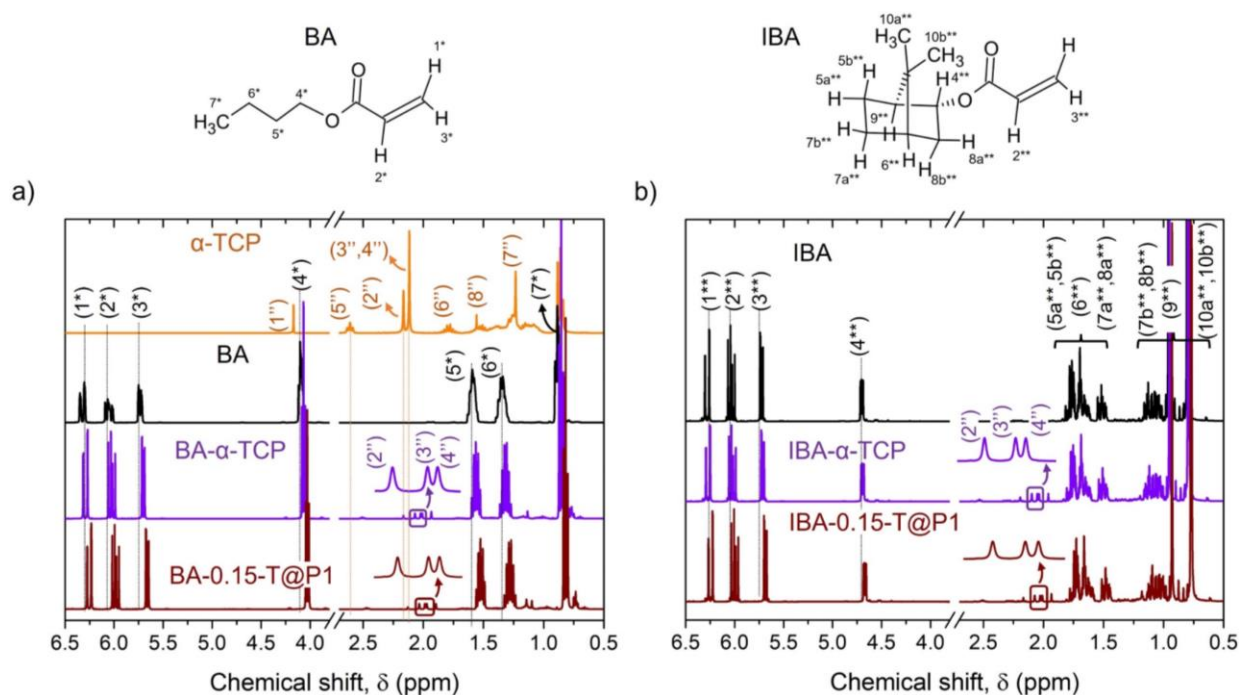

Figure S11. ^{1}H NMR spectra (CDCl$_3$, 400 MHz, 25 °C) of (a) BA and (b) IBA based combinations with and without the presence of α-TCP and 0.15-T@P1, respectively. Insets of Figure S11a,b shows characteristic NMR signals from CH$_3$ bonded to phenolic ring from α-TCP (2'',3'',4'').

To evaluate the hypothesis of opening ring by the acrylate monomer, a mixture with equimolar quantities of α-TCP and IBA were prepared and analyzed by ^{1}H NMR (Figure S12f). Varying the proportion between the compounds, it is possible to observe that the signal related CH$_3$ 2'', 3'', 4'' of α-TCP change from a singlet (Figure S12 c-f) to a doublet (Figure S12 a-b) in small concentration of α-TCP compared to IBA. The change in the multiplicity occurs when the relation between IBA:α-TCP is higher than 10. The result suggests that there is ideal condition to occur the activation of α-TCP, which in agreement with the PNCs stabilization.

^{13}C, HMBC and HSQC NMR analysis (Figure S13-S15) were also performed to better characterize the mixture (IBA-T@P). Comparing the spectra is possible to follow the modification on α-TCP signals in a sample with equimolar amount (Eq) of IBA-T@P (where the related CH$_3$ 2'', 3'', 4'' appear as singlet), and other in IBA in excess (where the related CH$_3$ 2'', 3'', 4'' appear as doublet). The ^{13}C and HSQC spectra (Figure S13-14) are focused on the signals that would supposedly undergo a modification in the chemical shift in an eventual opening ring, mainly the 5'', 6'', 7'', 8'' that are closer to the electrophilic sp^3 carbon. However, except the modification on signals intensity, no significant change

on chemical shift of those signals were observed. Nevertheless, the hypothesis of ring-opening reaction and an equilibrium shift between different α-TCP derivates species cannot be discarded.[15]
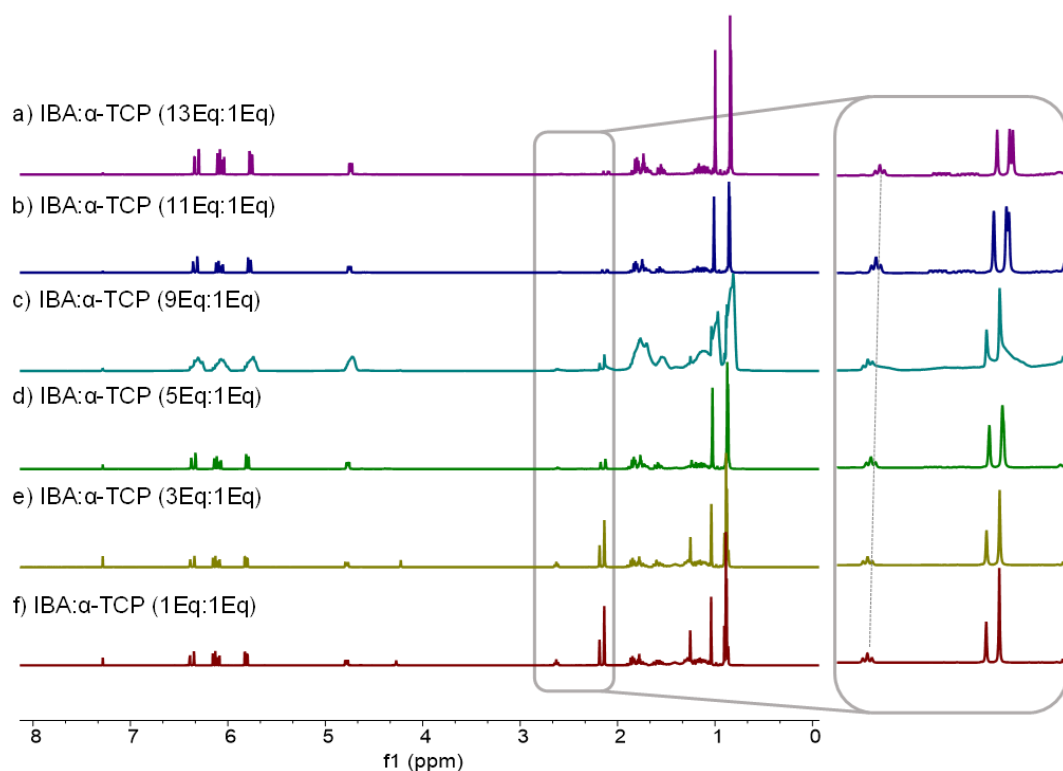

Figure S12. ^{1}H NMR spectra (CDCl$_3$, 400 MHz, 25 °C) of IBA-α-TCP in different IBA:α-TCP equimolar content ratio.
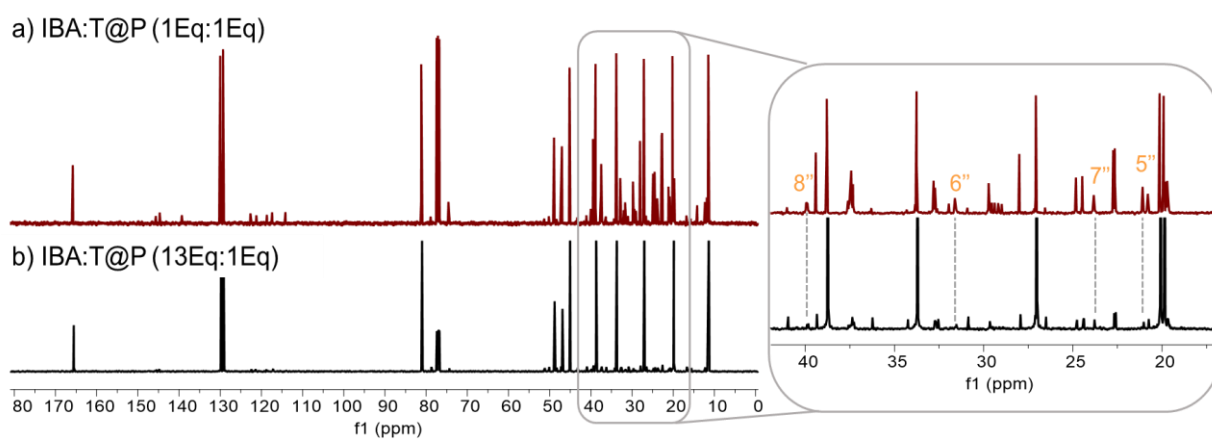

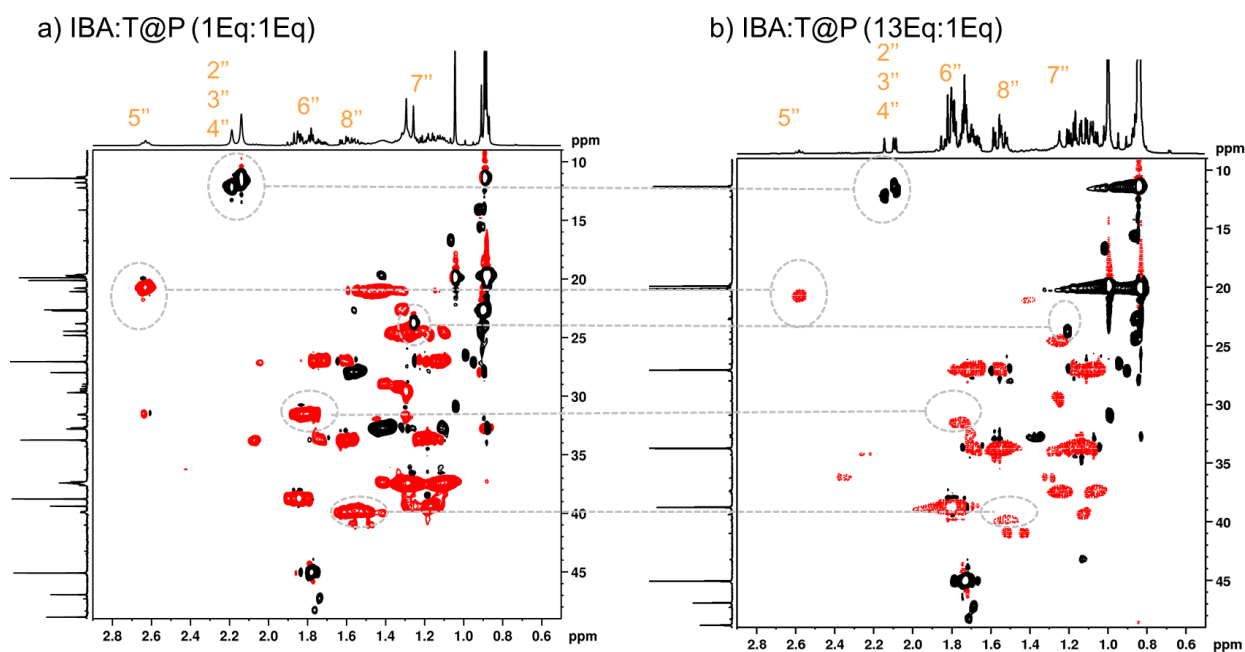**Figure S13.** ^{1}H,^{13}C-HMBC spectra expanded (CDCl$_3$, 400 MHz, 25 °C) of IBA:0.15-T@P1 with different equimolar content ratio.

Figure S14. $^1H,^{13}C$-HSQC spectra expanded (CDCl$_3$, 400 MHz, 25 °C) of IBA-T@P with different with different equimolar content ratio.
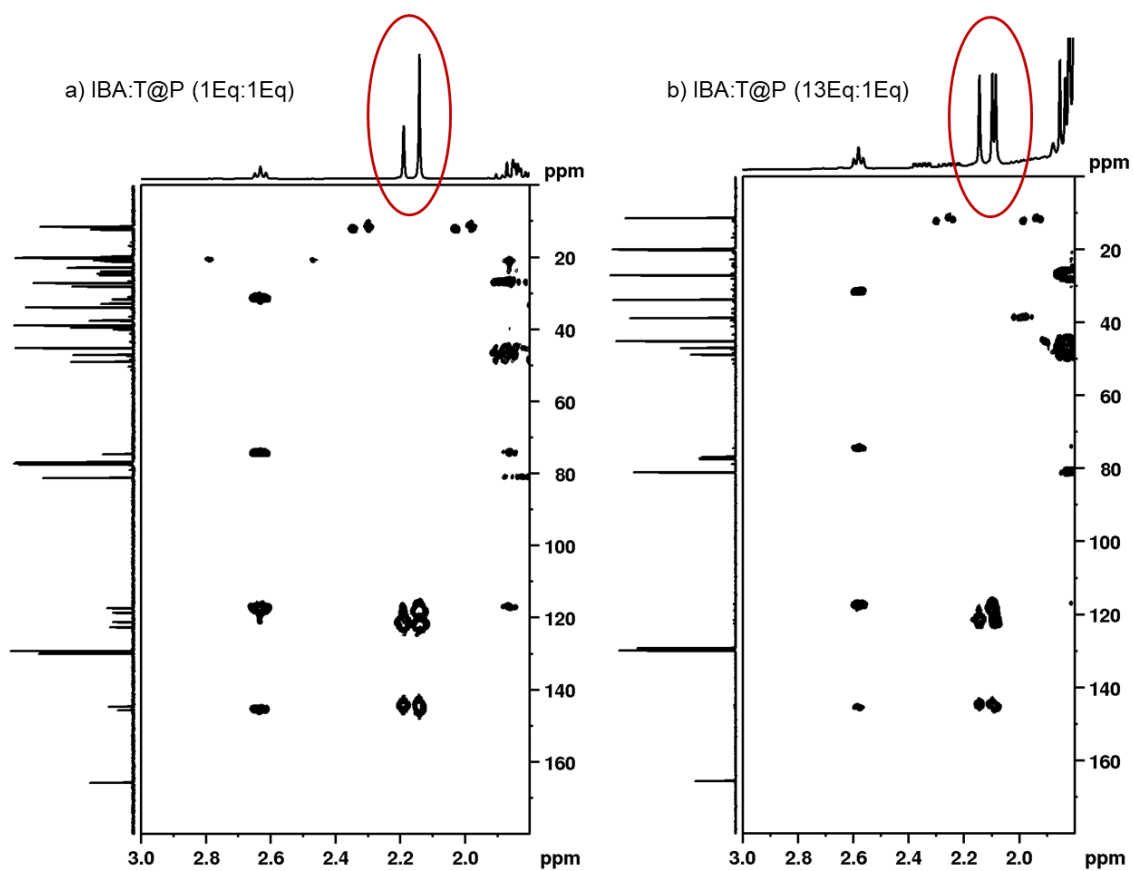

Figure S15. $^1H,^{13}C$-HMBC spectra expanded (CDCl$_3$, 400 MHz, 25 °C) of IBA-T@P with different concentrations.

References

[1]   E. Hassanabadi, M. Latifi, A. F. Gualdrón-Reyes, S. Masi, S. Y. joon, M. Poyatos, B. Julián-López, I. Mora Seró, *Nanoscale* **2020**, 12, 14194.

[2]   J. Hutter, M. Iannuzzi, F. Schiffmann, J. VandeVondele, *Wiley Interdisciplinary Reviews: Computational Molecular Science* **2014**, 4, 15.

[3]   C. Giansante, I. Infante, *The Journal of Physical Chemistry Letters* **2017**, 8, 5209.

[4]   J. P. Perdew, K. Burke, M. Ernzerhof, *Physical Review Letters* **1996**, 77, 3865.

[5]   O. Voznyy, S. M. Thon, A. H. Ip, E. H. Sargent, *The Journal of Physical Chemistry Letters* **2013**, 4, 987.

[6]   Y. Zhang, T. D. Siegler, C. J. Thomas, M. K. Abney, T. Shah, A. De Gorostiza, R. M. Greene, B. A. Korgel, *Chemistry of Materials* **2020**, 32, 5410.

[7]   S. Masi, A. F. Gualdrón-Reyes, I. Mora-Seró, *ACS Energy Letters* **2020**, 1974.

[8]   J.-K. Sun, S. Huang, X.-Z. Liu, Q. Xu, Q.-H. Zhang, W.-J. Jiang, D.-J. Xue, J.-C. Xu, J.-Y. Ma, J. Ding, Q.-Q. Ge, L. Gu, X.-H. Fang, H.-Z. Zhong, J.-S. Hu, L.-J. Wan, *Journal of the American Chemical Society* **2018**, 140, 11705.

[9]   X. Shen, Y. Zhang, S. V. Kershaw, T. Li, C. Wang, X. Zhang, W. Wang, D. Li, Y. Wang, M. Lu, L. Zhang, C. Sun, D. Zhao, G. Qin, X. Bai, W. W. Yu, A. L. Rogach, *Nano Letters* **2019**, 19, 1552.

[10]   R. Grisorio, M. E. Di Clemente, E. Fanizza, I. Allegretta, D. Altamura, M. Striccoli, R. Terzano, C. Giannini, M. Irimia-Vladu, G. P. Suranna, *Nanoscale* **2019**, 11, 986.

[11]   F. Liu, Y. Zhang, C. Ding, S. Kobayashi, T. Izuishi, N. Nakazawa, T. Toyoda, T. Ohta, S. Hayase, T. Minemoto, K. Yoshino, S. Dai, Q. Shen, *ACS Nano* **2017**, 11, 10373.

[12]   ChemicalBook, *https://www.chemicalbook.com/SpectrumEN_10191-41-0_1HNMR.htm (Accessed November 09, 2021).*

[13]   SDBS, *https://sdbs.db.aist.go.jp/sdbs/cgi-bin/direct_frame_top.cgi (accessed November 09, 2021).*

[14]   P. Glöckner, D. Schollmeyer, H. Ritter, *Designed Monomers and Polymers* **2012**, 5, 163.

[15]   F. Sarrami, A. A. Kroeger, A. Karton, *Chemical Physics Letters* **2018**, 708, 123.